Image Reconstruction using Simulated Annealing Algorithm in EIT

Ho-Chan Kim, Chang-Jin Boo, and Yoon-Joon Lee

Abstract: In electrical impedance tomography (EIT), various image reconstruction algorithms have been used in order to compute the internal resistivity distribution of the unknown object with its electric potential data at the boundary. Mathematically, the EIT image reconstruction algorithm is a nonlinear ill-posed inverse problem. This paper presents a simulated annealing technique as a statistical reconstruction algorithm for the solution of the static EIT inverse problem. Computer simulations with 32 channels synthetic data show that the spatial resolution of reconstructed images by the proposed scheme is improved as compared to that of the mNR algorithm at the expense of increased computational burden.

Keywords: Electrical impedance tomography, finite element method, inverse problem, simulated annealing.

1. INTRODUCTION

Electrical impedance tomography (EIT) plays an important role as an innovative monitoring tool for engineering applications such as biomedical imaging and process tomography due to its relatively cheap electronic hardware requirements and nonintrusive measurement property [1-3]. In EIT, different current patterns are injected to the unknown object through electrodes and the corresponding voltages are measured on its boundary surface. The physical relationship between inner resistivity (or conductivity) and boundary surface voltage is the generalized Laplace equation with appropriate boundary conditions. As such, it is impossible to obtain the closed-form solution for the resistivity distribution. Hence, the internal resistivity distribution of the unknown object is computed using the boundary voltage data based on various reconstruction algorithms.

Yorkey *et al.* [4] developed a modified Newton-Raphson (mNR) algorithm for a static EIT image reconstruction and compared it with other existing algorithms such as the backprojection, perturbation and double constraints methods. They concluded that the mNR reveals relatively good performance in terms of convergence rate and residual error compared to those of other methods. And yet, in real situations, the mNR method often fails to obtain satisfactory images from physical data due to large modeling error, poor signal to noise ratios (SNRs) and ill-conditioned (ill-posed) characteristics. That is, the ratio between the maximum and minimum eigenvalues of the information matrix (or Hessian matrix) is very large. In particular, the ill-conditioning of the information matrix results in an inaccurate matrix inverse so that the resistivity update process is very sensitive to the modeling and measurement errors.

The major difficulties in impedance imaging are in the nonlinearity of the problem itself and the poor sensitivity of the boundary voltages to the change of resistivity deep within the domain. Several researchers have suggested various element or mesh grouping methods where they force all meshes belonging to certain groups to have the same resistivity values [5,6].

Simulated annealing (SA) [7] is an optimization technique inspired from Monte Carlo methods in statistical mechanics. It attempts to avoid local optima by probabilistically taking non-locally optimal steps in the search space. The probability of taking such steps decreases with the "temperature" of the system, which in turn decreases with time. SA is able to deal with evaluation functions with rather arbitrary degrees of nonlinearities, discontinuities and stochasticity, and can process quite arbitrary boundary conditions and constraints imposed on these evaluation functions [7,8]. It has been shown that with a "large enough" initial temperature and a proper temperature schedule, SA guarantees a globally optimal solution [9].

In this paper, we will discuss the image reconstruction in EIT based on combining SA and

Manuscript received October 28, 2004; accepted February 22, 2005. Recommended by Editorial Board member Sun Kook Yoo under the direction of Editor Jin Bae Park. This work was supported by the Nuclear Academic Research Program by the Ministry of Science and Technology (MOST).

Ho-Chan Kim and Chang-Jin Boo are with the Department of Electrical Engineering, Cheju National University, 66 Jejudaehakno, Jeju-si, Jeju-do 690-756, Korea (e-mails: {hckim, boo1004}@cheju.ac.kr).

Yoon-Joon Lee is with the Department of Nuclear and Energy Engineering, Cheju National University, 66 Jejudaehakno, Jeju-si, Jeju-do 690-756, Korea (e-mail: leeyj@cheju.ac.kr).

mNR algorithms. We have divided the procedure for obtaining the internal resistivity distribution into two steps. In the first step, each mesh is classified into three mesh groups: target, background, and temporary groups. Following a few iterations of the mNR algorithm, an absolute value of meshes cannot be determined, but some useful information on the target images can be given. So, we use the mNR algorithm to determine the resistivity of meshes and rearrange the resistivity values of meshes by sorting them in ascending order. Then the boundary location between regions can be roughly decided and the mesh can be determined in relation to the target, background, or undetermined temporary group. In the second step, the values of these resistivities are determined using SA algorithm. This two-step approach allows us to better constrain the inverse problem and subsequently achieve a higher spatial resolution.

2. IMAGE RECONSTRUCTION USING SIMULATED ANNEALING ALGORITHM IN EIT

The numerical algorithm used to convert the electrical measurements at the boundary to a resistivity distribution is described here. The algorithm consists of iteratively solving the forward problem and updating the resistivity distribution as dictated by the formulation of the inverse problem. The forward problem of EIT calculates boundary potentials with the given electrical resistivity distribution, and the inverse problem of EIT takes potential measurements at the boundary to update the resistivity distribution.

2.1. The forward problem

When electrical currents $I_l (l = 1, \cdots, L)$ are injected into the object $\Omega \in R^2$ through electrodes $e_l (l = 1, \cdots, L)$ attached on the boundary $\partial\Omega$ and the resistivity distribution $\rho(x, y)$ is known over Ω, the corresponding induced electrical potential $u(x, y)$ can be determined uniquely from the generalized Laplace equation with Neumann boundary conditions. The complete electrode model takes into account both the shunting effect of the electrode and the contact impedances between the electrodes and the object. The equations of the complete electrode model are

$$\nabla \cdot (\rho^{-1} \nabla u) = 0 \text{ in } \Omega, \tag{1}$$

$$\begin{aligned} &\int_{e_l} \rho^{-1} \frac{\partial u}{\partial n} dS = I_l, \; l = 1, \cdots, L, \\ &u + z_l \rho^{-1} \frac{\partial u}{\partial n} = U_l \text{ on } e_l, \; l = 1, \cdots, L, \\ &\rho^{-1} \frac{\partial u}{\partial n} = 0 \text{ on } \partial\Omega \setminus \bigcup_{l=1}^{L} e_l, \end{aligned} \tag{2}$$

where z_l is the effective contact impedance between the l^{th} electrode and the object, U_l is the measured potential at the l^{th} electrode and n is the outward unit normal. In addition, we have the following two conditions for the injected currents and measured voltages by taking into account the conservation of electrical charge and appropriate selection of ground electrode, respectively.

$$\sum_{l=1}^{L} I_l = 0, \tag{3}$$

$$\sum_{l=1}^{L} U_l = 0. \tag{4}$$

The computation of the potential $u(x, y)$ for the given resistivity distribution $\rho(x, y)$ and boundary condition I_l is called the forward problem. The numerical solution for the forward problem can be obtained using the finite element method (FEM). In the FEM, the object area is discretized into small elements having a node at each corner. It is assumed that the resistivity distribution is constant within an element. The potential at each node is calculated by discretizing (1) into $YU_c = I_c$, where U_c is the vector of voltages at the FEM nodes and the electrodes, I_c is the vector of injected current patterns, and the matrix Y is a functions of the unknown resistivities.

2.2. The inverse problem

The inverse problem, also known as the image reconstruction, consists in reconstructing the resistivity distribution $\rho(x, y)$ from potential differences measured on the boundary of the object. Ideally, knowing the potential of the whole boundary makes the correspondence between the resistivity distribution and the potential biunique. The relatively simple situation depicted so far does not hold exactly in the real world. The methods used for solving the EIT problem search for an approximate solution, i.e., for a resistivity distribution minimizing some sort of residual involving the measured and calculated potential values. From a mathematical point of view, the EIT inverse problem consists in finding the coordinates of a point in a *M*-dimensional hyperspace, where M is the number of discrete elements whose union constitutes the tomographic section under consideration. In the past, several EIT image reconstruction algorithms for the current injection method have been developed by various authors. A review of these methods is given in [10]. To reconstruct the resistivity distribution inside the object, we have to solve the nonlinear ill-posed inverse problem. Regularization techniques are needed to

weaken the ill-posedness and to obtain stable solutions.

The Generalized Tikhonov regularized version of the EIT inverse problem can be written in the form [3]

$$\Psi(\rho) = \min\{\| U - V(\rho) \| + \lambda \| R\rho \|\}, \quad (5)$$

where $\rho \in R$ is the resistivity distribution. $V(\rho) \in R$ is the vector of voltages obtained from the model with known ρ, $U \in R$ are the measured voltages and R and λ are the regularization matrix and the regularization parameter, respectively. There are many approaches in the literature [11-14] to determine R and λ, but the usual choice is to fix $R = I$ with the identity matrix and to adjust λ empirically.

Minimizing the objective function $\Psi(\rho)$ gives an equation for the update of the resistivity vector

$$\begin{aligned} \rho_{k+1} &= \rho_k + \Delta\rho_{k+1}, \\ \Delta\rho_{k+1} &= (H_k + \lambda I)^{-1}\{J_k{}^T (U - V(\rho_k)) - \lambda\rho_k\}, \end{aligned} \quad (6)$$

where the partial derivative of Ψ with respect to ρ has been approximated by a Taylor series expansion around ρ_k. The Jacobian J_k is a matrix composed of the derivative of the vector of predicted potentials with respect to the unknown resistivities. The Jacobian is derived from the finite element formulation given by $J_k = \left.\frac{\partial\Psi}{\partial\rho}\right|_{\rho_k}$. The Hessian H_k is the second derivative of the predicted potentials with respect to the resistivity and is approximated as the square of the Jacobian for computational efficiency. Since the objective function $\Psi(\rho)$ is multimodal (i.e., it presents several local minima), the inversion procedure does not always converge to the true solution. The reconstruction algorithms are likely to be trapped in a local minimum and sometimes the best solution of a static EIT problem is rather unsatisfactory.

This paper attempts to apply SA to EIT image reconstruction. Two characteristics of SA algorithms appear to be of value in EIT reconstruction; no evaluation of function derivatives is needed and no assumption on function continuity needs to be made. The preceding considerations suggest the viability of employing SA's for the solution of the EIT problem, according to the procedure described in the following section.

2.3. The SA algorithm approach to EIT

In some applications like visualization of two-component systems, we may assume that there are only two different representative resistivity values; one resistivity value for the background and the other for the target. Here, the target need not be a single segment. It may be composed of multiple segments of the same resistivity value.

In this paper, we will discuss the image reconstruction in EIT using a two-step approach. We have divided the procedure for obtaining the internal resistivity distribution into two steps. In the first step, we adopted a mNR method as a basic image reconstruction algorithm. After a few initial mNR iterations performed without any grouping, we classified each mesh into one of three mesh groups: BackGroup (or TargetGroup) is the mesh group with the resistivity value of the background (or target). TempGroup is the group of meshes neither in BackGroup nor in TargetGroup. All meshes in BackGroup and in TargetGroup are forced to have the same but unknown resistivity value (ρ_{back} and ρ_{tar}), respectively. However, all meshes in TempGroup can have different resistivity values ($\rho_{temp,i}$, i=1,⋯,n_c-2).

The SA reconstruction algorithm for EIT can be formulated as follows. We will iteratively reconstruct an image that fits best the measured voltages U_l at the l th electrode. To do so, at each iteration we will calculate the pseudo voltages $V_l(\rho)$ that correspond to the present state of the reconstructed image. We assume that, by minimizing the difference between the measured voltages and the pseudo voltages, the reconstructed image will converge towards the sought-after original image. Therefore, we chose as cost function the following function of the relative difference between the computed and measured potentials on the object boundary

$$E(\rho) = \frac{1}{M_c}\sum_{i=1}^{M_c}\left(\frac{U_i - V_i(\rho)}{U_i}\right)^2, \quad (7)$$

where M_c is the total number of independent measurement.

SA starts with an initial schedule ρ_k and generates another schedule $\rho_{new} = \rho_k + \Delta\rho$ within a neighborhood. Let $E(\rho_k)$ and $E(\rho_{new})$ denote the energy (or cost) of schedules ρ_k and ρ_{new} respectively, which are calculated via objective function. In a minimization problem if $\Delta E = E(\rho_{new}) - E(\rho_k) < 0$ (i.e., ρ_{new} is better), then our new move (schedule) is accepted; otherwise, it is accepted with a probability of $P_r(i)$

$$P_r(i) = \exp\left(-\frac{\Delta E}{T_k}\right), \quad (8)$$

where T_k is the temperature at the k^{th} iteration. Note that as T_K decreases, the lower the probability to accept worse schedules. T_K is controlled by the cooling schedule function as given by (9)

$$T_k = \alpha T_{k-1}, \quad (9)$$

where $\alpha \in (0,1)$ is the temperature decay rate. The SA can be described with the following pseudo code using the notation.

SA algorithm in pseudo-code
Start
Select an initial resistivity distribution ρ_0
Select an initial temperature T_0
Select temperature reduction function
Select number of iterations for each temperature
Select number of temperatures
Repeat
  Set Temperature Counter = 0
  Repeat
    Set Iteration Counter = 0
    Generate solution ρ_{new}, ρ_{new} a neighborhood of ρ_k
    Calculate $\Delta E = E(\rho_{new}) - E(\rho_k)$
    If $\Delta E < 0$
      Then $\rho_{k+1} = \rho_{new}$
    Else
    Generate random value U uniformly in (0,1)
    If $U < \exp(-\Delta E / T_k)$ then $\rho_{k+1} = \rho_{new}$
    Iteration Counter = Iteration Counter +1
  Until number of iterations
  Counter Temperature = Counter Temperature +1
  Temperature $T_{k+1} = \alpha T_k$
Until number of temperatures
(stopping criterion, number of temperatures is satisfied)
ρ_k is the approximation to the optimal solution
End

SA requests that generic and problem specific decisions have to be made concerning algorithm parameters. The generic decisions involve the cooling schedule: initial temperature, final temperature and temperature reduction function. The problem-specific decisions include how to develop an initial solution and how to generate good neighbors to the current solution.

3. COMUTER SIMULATION

The proposed algorithm has been tested by comparing its results for numerical simulations with those obtained by the mNR method. For the current injection the trigonometric current patterns were used. For the forward calculations, the domain Ω was a unit disc and the mesh of 3104 triangular elements (M=3104) with 1681 nodes (N=1681) and 32 channels (L=32) was used as shown in Fig. 1(a). A different mesh system with 776 elements (M=776) and 453 nodes (N=453) was adopted for the inverse calculations as shown in Fig. 1(b). In this paper, under the assumption that the resistivity varies only in the radial direction within a cylindrical coordinate system [14], the results of the two inverse problem methods can be easily compared. The resistivity profile given to the finite element inverse solver varies from the center to the boundary of an object and is divided into 9 radial elements ($\rho_1, \cdots, \rho_9$) in Fig. 1(b).

Reasonable efforts were made to tune the SA parameters to enhance the performance of the algorithm. Standard stepwise temperature decay method is used. The initial temperature T_0 is 1 and the decay factor α is 0.8. Stopping criteria is based on the number of temperatures. The number of temperatures used is 50.

Resolution of the method is determined by a number of variables including resistivity contrast and distribution, position within the domain, and even current patterns. The ability to positively distinguish between two similar resistivity distributions also depends upon the precision of the voltage measurements. These factors necessitate caution when designing an experiment and interpreting results. Therefore, to verify the appropriateness of EIT for this application, a computational experiment was conducted.

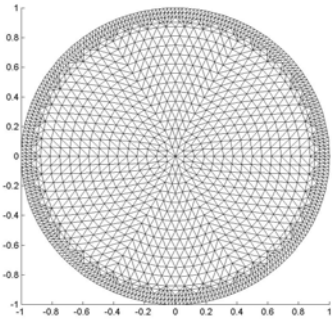

(a)

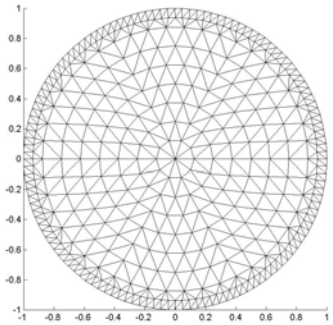

(b)

Fig. 1. Finite element mesh used in the calculation (The resistivities of the elements within an annular ring are identical.) (a) mesh for forward solver, (b) mesh for inverse solver.

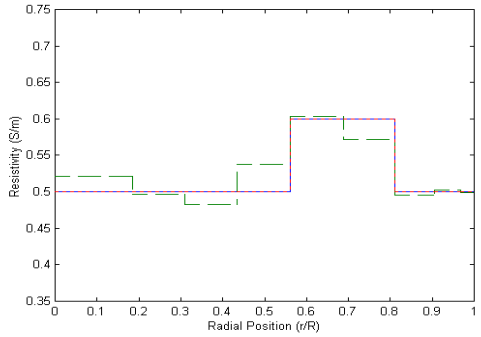

Fig. 2. True resistivities (solid line) and computed resistivities using mNR (dash line) and SA (dotted line).

Synthetic boundary potentials were computed for idealized resistivity distributions using the finite element method described earlier. The boundary potentials were then used for inversion and the results were compared to the original resistivity profiles. The resistivity profile appearing in Fig. 2 contains two large discontinuities in the original resistivity distribution. The present example is a severe test in EIT problems because there are large step changes at r/R =0.56 and 0.81 preventing electric currents from going into the center region.

We started a few mNR iterations without any mesh grouping with a homogeneous initial guess. In Table 1, we see that the mNR algorithm may roughly estimate the given true resistivities. Since the mNR have a large error at the boundary of target and background in Fig. 2, we cannot obtain reconstructed images of high spatial resolution. This kind of poor convergence is a very typical problem in NR-type algorithms.

However, we can significantly improve the mNR's poor convergence by adopting the proposed SA via a two-step approach as follows. In the first step, we adopted a mNR method as a basic image reconstruction algorithm. After a few initial mNR iterations performed without any grouping, we rearrange the resistivity values of meshes by sorting them in ascending order. Then the boundary location between regions can be roughly decided and the mesh can be determined to the target, background, or undetermined temporary group. In this paper, from Table 1, 2 meshes (ρ_5, ρ_6) and 5 meshes ($\rho_2, \rho_3, \rho_7, \rho_8, \rho_9$) among 9 may be grouped to TargetGroup (ρ_{tar}) and BackGroup (ρ_{back}), respectively. The remainders of meshes (ρ_1, ρ_4) are grouped to TempGroup. Hence, the number of unknowns is reduced to 4.

In the second step, after mesh grouping, we will determine the values of these resistivities using SA algorithm. The SA solves the EIT problem, searching for the resistivities (ρ_1, ρ_4 , ρ_{tar} and ρ_{back}) and minimizing the reconstruction error. In this case, we will use ρ_{back} (or ρ_{tar}) as the minimum (or maximum) values of the unknown resistivity distribution. The computed resistivities in SA are constrained between the minimum and maximum values. The initial values of unknown ρ_{tar} and ρ_{back} are the average resistivity values of meshes in the BackGroup and TargetGroup, respectively. From Fig. 2 and Table 1, the inverted profile using SA matches the original profile very well near the wall at r/R =1.0 as well as the center at r/R =0.0. Furthermore, the SA reconstruction is practically perfect for the jump of resistivity at *r/R*=0.56 and 0.81.

Table 1. True resistivities and computed resistivities using mNR and SA.

	ρ_1	ρ_2	ρ_3	ρ_4	ρ_5	ρ_6	ρ_7	ρ_8	ρ_9
Real	0.5	0.5	0.5	0.5	0.6	0.6	0.5	0.5	0.5
mNR	.521	.495	.488	.537	.598	.564	.496	.502	.500
SA	.500	.500	.500	.500	.600	.600	.500	.500	.500

4. CONCLUSION

In this paper, an EIT image reconstruction method based on SA via a two-step approach was presented to improve the spatial resolution. A technique based on SA algorithm with the knowledge of mNR was developed for the solution of the EIT inverse problem. Although SA is expensive in terms of computing time and resources, which is a weakness of the method that renders it presently unsuitable for real-time tomographic applications, the exploitation of *a priori* knowledge will produce very good reconstructions. Further extensions include an EIT image reconstruction to multi-resistivity value problems.

REFERENCES

[1] J. G. Webster, *Electrical Impedance Tomography*, Adam Hilger, 1990.

[2] J. C. Newell, D. G. Gisser, and D. Isaacson, "An electric current tomograph," *IEEE Trans. on Biomedical Engineering*, vol. 35, no. 10, pp. 828-833, 1987.

[3] M. Vauhkonen, *Electrical Impedance Tomography and Priori Information*, Kuopio University Publications Co., Natural and Environmental Sciences 62, 1997.

[4] T. J. Yorkey, J. G. Webster, and W. J. Tompkins, "Comparing reconstruction algorithms for electrical impedance tomography," *IEEE Trans. on Biomedical Engineering*, vol. 34, no. 11, pp. 843-852, 1987.

[5] M. Glidewell and K. T. Ng, "Anatomically constrained electrical impedance tomography for anisotropic bodies via a two-step approach,"

IEEE Trans. on Medical Imaging, vol. 14, no. 3, pp. 498-503, 1995.

[6] K. D. Paulsen, P. M. Meaney, M. J. Moskowitz, and J. M. Sullivan, "A dual mesh scheme for finite element based reconstruction algorithm," *IEEE Trans. on Medical Imaging*, vol. 14, no. 3, pp. 504–514, 1995.

[7] S. Kirkpatrick, C. D. Gelatt, and M. P. Vecchi, "Optimization by simulated annealing," *Science*, vol. 220, pp. 671-680, 1983.

[8] L. Ingber, "Simulated annealing: Practice and theory," *Journal of Mathematical Computation Modelling*, vol. 18, no. 11, pp. 29-57, 1993

[9] S. Gemen and D. Geman, "Stochastic relaxation, Gibbs distribution and the Bayesian restoration in images," *IEEE Trans. on Pattern Analysis and Machine Intelligence*, vol. 6, no. 3, pp. 721-741, 1984.

[10] T. Murai and Y. Kagawa, "Electrical impedance computed tomography based on a finite element model," *IEEE Trans. on Biomedical Engineering*, vol. 32, no. 3, pp. 177-184, 1985.

[11] C. Cohen-Bacrie, Y. Goussard, and R. Guardo, "Regularized reconstruction in electrical impedance tomography using a variance uniformization constraint," *IEEE Trans. on Medical Imaging*, vol. 16, no. 5, pp. 170-179, 1997.

[12] M. Vauhkonen, D. Vadasz, P. A. Karjalainen, and J. P. Kaipio, "Subspace regularization method for electrical impedance tomography," *Proc. of 1st International Conference on Bioelectromagnetism*, Tampere, Finland, pp. 9-13, 1996.

[13] A. Adler and R. Guardo, "Electrical impedance tomography: regularized imaging and contrast detection," *IEEE Trans. on Medical Imaging*, vol. 15, no. 2, pp. 170-179, 1996.

[14] C. J. Grootveld, A. Segal, and B. Scarlett, "Regularized modified Newton-Raphson technique applied to electrical impedance tomography," *International Journal of Imaging System Technology*, vol. 9, pp. 60-65, 1998.

[15] M. C. Kim, S. Kim, K. Y. Kim, J. H. Lee, and Y. J. Lee, "Reconstruction of particle concentration distribution in annular Couette flow using electrical impedance tomography," *Journal of Industrial and Engineering Chemistry*, vol. 7, no. 5, pp. 341-347, 2001.

Ho-Chan Kim received his B.S., M.S., and Ph.D. degrees in Control and Instrumentation Engineering from Seoul National University, Korea, in 1987, 1989, and 1994, respectively. He was part of the research staff at the Korea Institute of Science and Technology (KIST) from 1994 to 1995. Since then, he has been with the Department of Electrical Engineering at Cheju National University, where he is currently an Associate Professor. He was a Visiting Scholar at Pennsylvania State University from 1999 to 2000. His research interests include robust adaptive control, wind control, and power control.

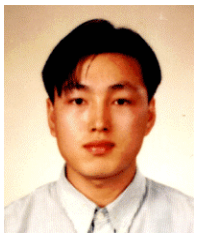

Chang-Jin Boo received his B.S. and M.S. in Electrical Engineering from Cheju National University, Korea, in 2001 and 2003 respectively. He is currently a Ph.D. student at Cheju National University. His research interests include embedded and RT system control.

Yoon-Joon Lee received his B.S. (Seoul National Univ., 1975), M.S. (Penn State Univ., 1980), and Ph.D. degree (Seoul National Univ., 1990) all in Nuclear Engineering. He worked as a Nuclear Engineer from 1975 to 1978, and has 8 years experience in plant design. He has been working in the Department of Nuclear and Energy Engineering at Cheju National University since 1984. His major interest is the automatization of nuclear plant operations.